ACS APPLIED MATERIALS & INTERFACES

university of groningen

Subscriber access provided by University of Groningen

Organic Electronic Devices

Significance of Dopant/Component Miscibility to Efficient N-Doping in Polymer Solar Cells

Yabing Tang, Baojun Lin, Hanzhang Zhao, Tao Li, Wei Ma, and Han Yan

ACS Appl. Mater. Interfaces, **Just Accepted Manuscript** • DOI: 10.1021/acsami.9b21252 • Publication Date (Web): 21 Feb 2020

Downloaded from pubs.acs.org on February 22, 2020

Just Accepted

"Just Accepted" manuscripts have been peer-reviewed and accepted for publication. They are posted online prior to technical editing, formatting for publication and author proofing. The American Chemical Society provides "Just Accepted" as a service to the research community to expedite the dissemination of scientific material as soon as possible after acceptance. "Just Accepted" manuscripts appear in full in PDF format accompanied by an HTML abstract. "Just Accepted" manuscripts have been fully peer reviewed, but should not be considered the official version of record. They are citable by the Digital Object Identifier (DOI®). "Just Accepted" is an optional service offered to authors. Therefore, the "Just Accepted" Web site may not include all articles that will be published in the journal. After a manuscript is technically edited and formatted, it will be removed from the "Just Accepted" Web site and published as an ASAP article. Note that technical editing may introduce minor changes to the manuscript text and/or graphics which could affect content, and all legal disclaimers and ethical guidelines that apply to the journal pertain. ACS cannot be held responsible for errors or consequences arising from the use of information contained in these "Just Accepted" manuscripts.

is published by the American Chemical Society. 1155 Sixteenth Street N.W., Washington, DC 20036

Published by American Chemical Society. Copyright © American Chemical Society. However, no copyright claim is made to original U.S. Government works, or works produced by employees of any Commonwealth realm Crown government in the course of their duties.

Significance of Dopant/Component Miscibility to Efficient N-Doping in Polymer Solar Cells

Yabing Tang,[†] Baojun Lin,[†] Hanzhang Zhao,[‡] Tao Li,[‡] Wei Ma,[,†] Han Yan[*,†]*

[†]State Key Laboratory for Mechanical Behavior of Materials, Xi'an Jiaotong University, Xi'an 710049, P. R. China

[‡]Center of Spintronics and Quantum Systems, State Key Laboratory for Mechanical Behavior of Materials, School of Materials Science and Engineering, Xi'an Jiaotong University, Xi'an, China

KEYWORDS：Molecular doping, n-doping, polymer solar cell, doped morphology, ternary phase diagram

TOC:

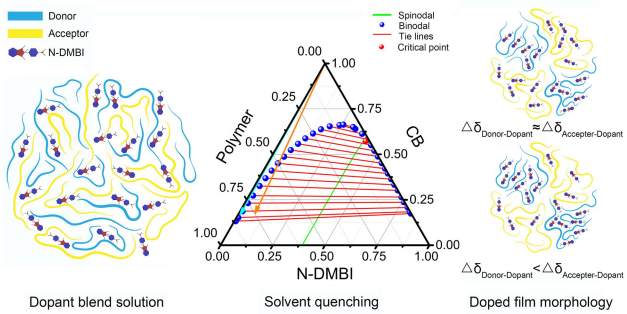

ABSTRACT: The uncertain dopant location in the bulk heterojunction (BHJ) film hinders the wide application of molecular doping in polymer solar cells (PSCs) as is in other organic devices. It is known that the interaction between dopant and component governs the dopant distribution in the BHJ film, and thus largely controls the effectiveness of molecular doping. After excluding the strong dopant/component interaction by forming the charge-transfer complex in solution, we estimate the dopant/component miscibility by calculating the difference of Hansen's total solubility parameters ($\triangle\delta_{i\text{-}Hansen}$) and prove its correctness by contact angle measurements, and two model systems of poly[(2,6-(4,8-bis(5-(2-ethylhexyl)thiophe-2-yl)-benzo[1,2-b:4,5-b']dithiophene))-alt-(5,5-(1',3'-di-2-thienyl -5',7'-bis(2-ethylhexyl)benzo[1',2'-c:4',5'-c']dithiophene-4,8-dione))] (PBDB)/poly{[N,N'-bis(2-octyldodecyl)-naphthalene-1,4,5,8-bis(dicarboximide)-2,6-diyl]-alt-5,5'-(2,2'-bithiophene)} (N2200) and poly[4,8-bis(5-(2-ethylhexyl)-thiophene-2-yl)benzo[1,2-b;4,5-b']dithiophene-2,6-diyl-alt-(4-(2-ethylhexyl)-3-fluorothieno[3,4-b]thiophene-)-2-carboxylate-2-6-diyl]] (PCE10)/N2200 are selected to reveal the miscibility-photovoltaic performance relations. Only the material combination with large $\triangle\delta_{i\text{-}Hansen}$ between n-dopant (4-(1,3-dimethyl-2,3-dihydro-1H-benzoimidazol-2-yl) phenyl) dimethylamine (N-DMBI) and the donor polymer achieves enhanced photovoltaic performance. After that, we examine the doped morphology of polymer blends. Since the polymers' crystallizations are negatively affected by N-DMBI addition, we ensure the significance of n-doping on the enhanced device performance. Besides the dopant/polymer interaction, the solvent/polymer and solvent/dopant interactions are also considered to evaluate the kinetic effect on N-DMBI distribution by drawing the ternary phase diagram. We conclude that the kinetic morphological evolution doesn't change the miscibility governed N-DMBI distribution in the BHJ film. Finally, we provide a direct relationship between the N-DMBI position and the device

property by fabricating the bi-layer devices. The enhancement of photovoltaic performances is observed in both of material systems only if the N-DMBI distributes in N2200. Our work outlines a basis for using the dopant/component interaction and ternary phase diagram to predict the dopant distribution before extensive experiments. It significantly reduces the trial-to-error work and increases the reliability of molecularly doped PSCs.

INTRODUCTION

PSC is a potentially attractive photovoltaic technology. The efficient PSCs are based on BHJ structure, which consists the bi-continuous network of electron-donor and electron-acceptor materials.[1-2] During the past years, PSCs have made great progress in power conversion efficiency (PCE) due to the development of non-fullerene acceptors. Nowadays, certified PCE value over 16% has been reported for single junction device.[3] To achieve better performance, the photo-charge generating and transporting processes need to be improved to further decrease the losses of photovoltaic parameters. Comparing with the presently used strategies such as materials synthesis,[4-6] morphology optimization,[7-9] and interlayer design,[10-12] molecular doping is an attractive concept which aims at directly tuning the optoelectronic properties of organic semiconductors including the charge distribution,[13-15] carrier mobility,[16-18] and trap density etc.[19-22] The systematic studies of BHJ doped PSCs started in 2011.[23] Fundamental studies reveal that molecular doping potentially improves the photovoltaic performances by facilitating the exciton splitting,[23-24] suppressing the carrier recombination,[23, 25-27] and optimizing the BHJ morphology.[28-29] Yet those studies mainly focused on p-doping in donor materials, developing the equally important n-doping in non-fullerene acceptors becomes urgent in future studies.[30]

According to the summary by Lin et al., the air-stable, solution processed n-dopants mainly involve two classes of materials, including the hydride-reduction of stable organic cations and tetraalkylammonium salts of simple inorganic ions.[31] Unlike the restricted ionization potential (IP) in p-dopants, such as 2,3,5,6-tetrafluoro-7,7,8,8-tetracyanoquinodimethane (F4TCNQ),[32] n-dopants possess sufficient doping strength due to the radical anions. Taking N-DMBI for example, it effectively dopes materials with lowest unoccupied molecular orbit (LUMO) levels ranging from 3.0 to 3.9 eV.[31] Thus the main obstacle to the efficient n-doping in PSCs is the dopant distribution in the BHJ film. The n-dopants ideally distribute solely with the acceptors, incorrect dispersion in donors will reduce or even negatively affect the doping effect.[33-34] However, the weak van der Waals interactions between the dopant and component, together with the ultralow doping content (usually less than 0.1 wt%), inhibit the prediction and observation of dopant distribution in the BHJ film. Inspired by recent studies on BHJ blend films, where the phase separation and phase purity are estimated by the components' miscibility according to the Flory-Huggins theory, [35-37] the dopant distribution can be inferred by comparing its miscibility with each component in the BHJ film. This methodology enables us to relate the dopant/component miscibility with the photovoltaic performances in n-doped PSCs.

We selected two polymer/polymer material systems with the same polymer acceptor-N2200. Polymer donors are different in miscibility with n-dopant, N-DMBI, which produces various extent of n-dopant distribution in polymer donor and polymer acceptor domains. Photovoltaic testing revealed that higher short-circuit current (J_{sc}) will be achieved when N-DMBI is less miscible with polymer donors. Thorough studies by morphology and crystalline analysis excluded the role of morphological modifier of N-DMBI in the BHJ film, and we confirmed the electronic n-doping as the reason for J_{sc} enhancement. The N-DMBI distribution in respective

BHJ films was further simulated by calculating the solvent contained ternary phase diagram, which allows us to discuss the N-DMBI distribution with regard to the kinetic morphological evolution. After analyzing the effects of phase separation time and solvent/polymer interaction related polymer mobility, we conclude that the kinetic morphological evolution doesn't alter the miscibility driven N-DMBI distribution in the BHJ film. The dopant distribution is further proved by fabricating the planar heterojunction (PHJ) devices where we confined the N-DMBI in each single layer. In accordance with our expectation, the J_{sc} enhancement was observed in both of PCE10/N2200 and PBDB-T/N2200 systems only if N-DMBI located in the N2200 layer. Our studies demonstrate the electronic n-doping as an efficient and general approach to improve the PCE in PSCs. The pre-requisition for efficient n-doping is poor miscibility between the dopant and donor to guarantee favored dopant distribution.

RESULTS AND DISCUSSION

In this work, all-polymer material systems PCE10/N2200 and PBDB-T/N2200 were adopted for our investigation, and a typical n-dopant N-DMBI was used to dope N2200 (**Figure 1a**). The n-doping effect was confirmed by the increased surface potential measured by Kelvin probe force microscopy (KPFM) when adding N-DMBI into the N2200 film (**Figure S1**). According to Moulé's reports, the dopant distribution in semiconducting polymer film was pre-determined in solution.[38] The formation of charge-transfer complex (CTC) in solution provided strong dopant/component binding, and this led to the highly selective dopant distribution in the multi-phase blend film. Thus we examined the CTC products by the absorption spectrum of polymer solutions. In **Figure 1b** and **c**, we observed no CTC peaks after N-DMBI addition. Under this weak doping situation, most dopants disperse in amorphous polymer regions,[39] and their distribution in the BHJ film is driven by the dopant/component miscibility during film formation.

The miscibility between N-DMBI and the polymer was evaluated by the Hansen's total solubility parameters ($\delta_{i\text{-Hansen}}$) via theoretical calculation and verified by contact angle measurements (**Figure 1d-f and Figure S2**). The calculated and measured values of δ are summarized in **Table S1.** The two independent groups of data demonstrate the same order of dopant/component miscibility. The smaller difference in the value of solubility parameter ($\triangle\delta$) demonstrates better dopant/component miscibility. Taking the calculated $\delta_{i\text{-Hansen}}$ for example, the $\triangle\delta_{i\text{-Hansen}}$ between N-DMBI and N2200 is 3.5 $MPa^{1/2}$, which is comparable to the value of 2.7 $MPa^{1/2}$ between N-DMBI and PCE10. Since N-DMBI/PBDB-T has the smallest $\triangle\delta_{i\text{-Hansen}}$ of 1.0 $MPa^{1/2}$, more N-DMBI tend to distribute in the PBDB-T domains in the BHJ blend film. Accordingly, we deduce that the N-DMBI doping is more efficient in the PCE10/N2200 BHJ film.

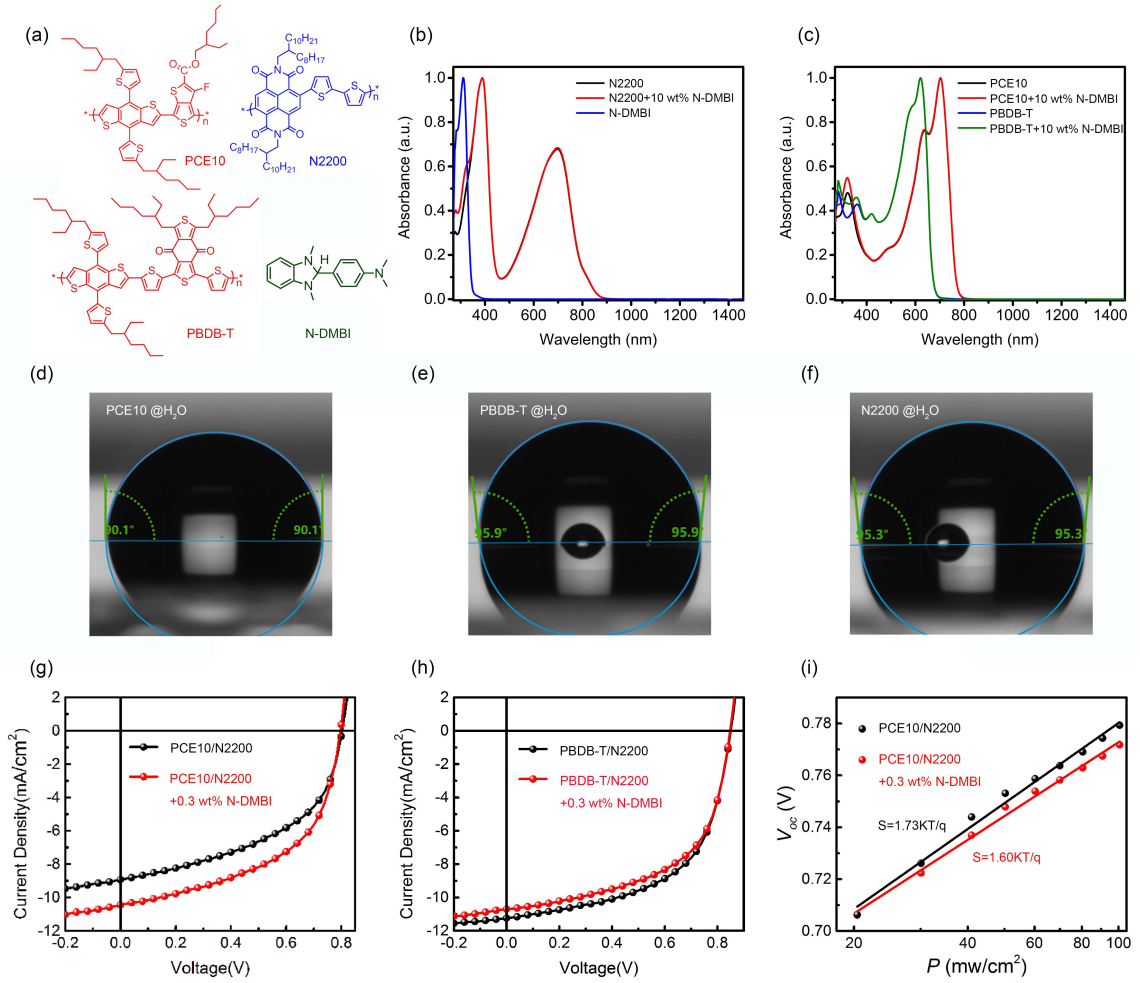

Figure 1. (a) The molecular structures of PCE10, PBDB-T, N2200, and N-DMBI. (b) The normalized absorbance of N2200, 10 wt% N-DMBI doped N2200 and N-DMBI solutions. (c) The normalized absorbance of PCE10, PBDB-T and their corresponding 10 wt% N-DMBI doped solutions. (d-f) Contact angle measurements of PCE10, PBDB-T, and N2200. (g) *J-V* curves of PCE10/N2200 BHJ devices. (h) *J-V* curves of PBDB-T/N2200 BHJ devices. (i) Dependence of V_{oc} on light intensity for PCE10/N2200 BHJ devices.

Table 1. Photovoltaic performance of PSCs with various N-DMBI contents.[a]

Materials		$V_{oc\ max}$ (V)	FF $_{max}$ (%)	$J_{sc\ max}$ (mA/cm^2)	$J_{sc\ avg}$ (mA/cm^2)	PCE$_{max}$ (%)	PCE$_{avg}$ (%)
N-DMBI in PCE10/N2200	Control	0.80	46.5	9.4	9.4±0.1	3.5	3.4±0.1
	0.05 wt%	0.79	45.7	9.9	9.5±0.3	3.6	3.5±0.1
	0.1 wt%	0.80	51.2	9.8	9.7±0.1	4.0	4.0±0.0
	0.3 wt%	0.80	52.3	10.4	10.3±0.1	4.4	4.2±0.1
	0.5 wt%	0.80	48.9	10.3	10.0±0.2	4.0	3.8±0.1
	1 wt%	0.74	41.4	6.2	5.9±0.2	1.9	1.8±0.0

N-DMBI in PBDB-T/N2200	Control	0.85	56.7	11.2	11.1±0.2	5.5	5.4±0.1
	0.05 wt%	0.85	56.2	11.2	11.0±0.3	5.4	5.3±0.1
	0.1 wt%	0.85	56.9	11.1	10.8±0.3	5.3	5.3±0.0
	0.3 wt%	0.85	56.2	10.7	10.6±0.3	5.2	5.1±0.0
	0.5 wt%	0.85	56.0	10.4	10.4±0.2	5.0	4.9±0.1
	1 wt%	0.74	38.3	5.4	4.9±0.3	1.5	1.5±0.1

[a] Average J_{sc} and PCE of 10 devices fabricated under identical conditions $\pm$1 standard deviation.

We fabricated photovoltaic devices in inverted structure to test the N-DMBI doped BHJ devices. The film thicknesses are 100±10nm and 80±10nm for PCE10/N2200 and PBDB-T/N2200 blends, respectively. PSC devices were characterized under AM 1.5 G illumination. The detailed data including the J_{sc}, open-circuit voltage (V_{oc}), fill factor (*FF*), and PCE are summarized in **Table 1**. It is impressive that the J_{sc} rises from 9.4 mA/cm^2 to 10.4 mA/cm^2 simultaneously with *FF* enhancement from 46.5% to 52.3% when 0.3 wt% N-DMBI is added in the PCE10/N2200 film (**Figure 1g**). In contrast to this, we observe slight J_{sc} decay in the PBDB-T/N2200 material system (**Figure 1h**). The J_{sc} variations are consistent with the external quantum efficiency (EQE) measurement, where the integrated current density demonstrates a J_{sc} enhancement of 1.0 mA/cm^2 and a slight decrease of 0.4 mA/cm^2 when adding equal content of 0.3 wt% N-DMBI to PCE10/N2200 and PBDB-T/N2200 films (**Figure S3**). The photovoltaic performances well support our assumption that the efficient n-doping requires worse miscibility between n-dopant and polymer donor in the BHJ film. Plotting V_{oc} on the natural logarithm of light intensity, we obtain the device physics in the n-doped PCE10/N2200 BHJ films. The V_{oc} slope decreases from 1.73 kT/q to 1.60 kT/q with addition of 0.3 wt% N-DMBI (**Figure 1i**), which was ascribed to trap-filling in our published study.[25]

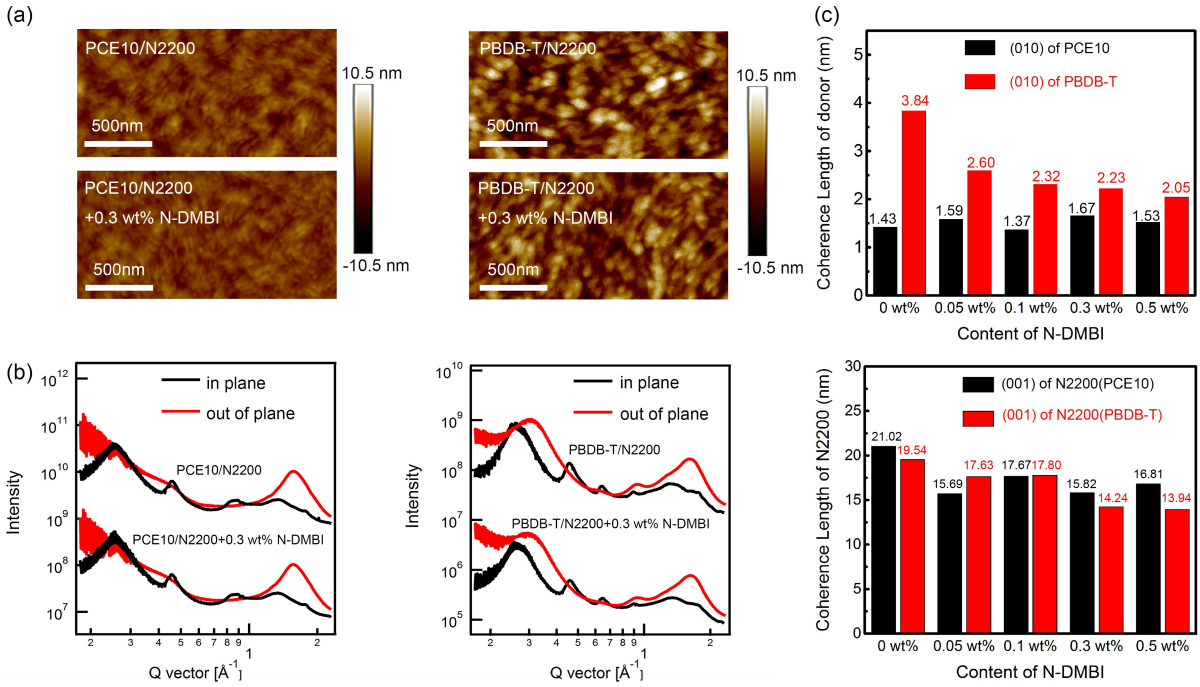

Figure 2. (a) TM-AFM images of the control and 0.3 wt% N-DMBI doped BHJ films: the left panel is PCE10/N2200 image and the right panel is PBDB-T/N2200 image. (b) In plane and out of plane line cuts of the control and 0.3 wt% N-DMBI doped BHJ films. (c) Corresponding histograms of the fitted coherence length of donor polymers and N2200 according to Scherrer equation.

According to the previous reports, the enhancement of photovoltaic performance may come from the morphologic optimization. [28-29] To clarify the role of N-DMBI here, the morphology of the control and 0.3 wt% N-DMBI doped BHJ films are characterized by tapping-mode atomic force microscope (TM-AFM) and grazing incident wide-angle X-ray scattering (GIWAXS) in series.[40] We observe smaller values of root-mean-square (RMS) in doped films for both material systems (from 1.26 to 1.03 nm in PCE10/N2200, and from 2.96 to 2.47 nm in PBDB-T/N2200), which implies the disruption of polymer stacking with addition of 0.3 wt% N-DMBI. GIWAXS was performed to reveal the impacts of N-DMBI on molecular orientation and stacking in both systems. Comparing the peak intensity in two-dimensional directions (**Figure 2b**, **Figure S4** and **Figure S5**), face-on orientation is more favored in PCE10/N2200, while PBDB-T/N2200 composes mixture of face-on and edge-on domains. In spite of different polymer stacking modes,

the addition of 0.3 wt% N-DMBI doesn't alter the polymer orientation in blend films. The peak positions also don't change with N-DMBI doping, demonstrating the absence of dopant/polymer co-crystalline phases according to Salleo's reports.[39, 41] This agrees with the results in **Figure 1b** and **c**, and supports our assumption that the dopant distribution in the blend film is determined in the film formation process rather in solution. The stacking order is estimated by fitting the coherence length (CL) of the scattering profiles. The CL of PBDB-T decreases with N-DMBI addition while the CL of PCE10 keeps constant according to the (010) peak at 1.69 $Å^{-1}$ and 1.60 $Å^{-1}$ respectively. Meanwhile, the molecular order of N2200 is evaluated by fitting its (001) peak at 0.46 $Å^{-1}$. The corresponding values of CL decay in both systems. On the basis of above analysis, we state that the addition of N-DMBI disrupts the molecular ordering in both of polymer blend films, thus the electronic n-doping is responsible for the performance improvement here.

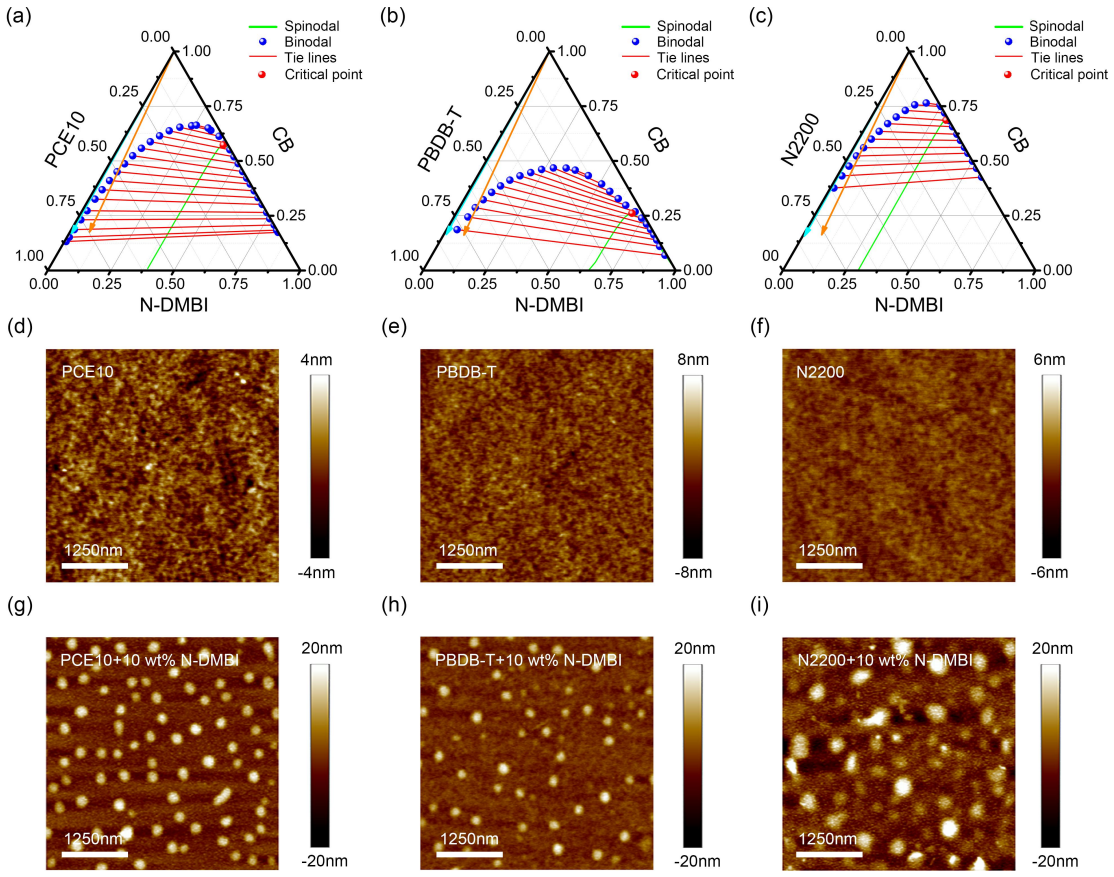

Figure 3. (a-c) Ternary phase diagrams of solvent/polymer/dopant material combinations: (a) CB/PCE10/N-DMBI, (b) CB/PBDB-T/N-DMBI, and (c) CB/N2200/N-DMBI. The region inside the spinodal line is of complete instability; the binodal line is the boundary between the single phase region and the metastable region; the tie lines connect the compositions with equal chemical potentials; the critical point is the intersection of both the binodal line and the spinodal line; the colored arrows are the solvent quenching lines, indicting the compositional variation of blend solution during solvent quenching: the blue one represents the mass ratio of 100:1 for polymer: N-DMBI, and the orange one represents the mass ratio of 10:1 for polymer: N-DMBI. (d-f) CM-AFM images of neat PCE10, PBDB-T and N2200 films. (g-i) CM-AFM images of 10 wt% N-DMBI doped PCE10, PBDB-T and N2200 films.

To lend more support to the miscibility related n-doping effect on photovoltaic performances, the kinetic factors on the evolution of doped morphology during film formation need to be taken into account. For clarity, we studied the phase behaviors of N-DMBI with distinct polymers. Taking chlorobenzene (CB) as the solvent, we calculated the ternary phase diagrams based on the Flory-Huggins theory via calculated Hansen's total solubility parameters (**Figure 3a-c**),[42-45] and the ternary phase diagrams drawn by separated Hansen solubility parameters are also

displayed in **Figure S6**. The molecular weights of PCE10, PBDB-T and N2200 measured by gel permeation chromatography (GPC) are around 120, 68 and 185 kDa (**Figure S7**), respectively. All parameters for the theoretical calculations are summarized in **Table S2**, and the details are given in the Supporting Information. In all cases of our experiment, the solvent quenches through the region between the binodal and spinodal lines, thus the L-L phase separation develops via droplet collision in this meta-stable region. Keep the knowledge in mind, the morphology of doped polymer films can be deduced by simultaneously considering the effects of phase separation time and the polymer mobility. We evaluate the initial time for L-L phase separation by the intersection of solvent quenching line and binodal line. The L-L phase separation occurs in the order of N2200, PCE10, and PBDB-T (**Figure 3a-c**), in accordance with the polymer/N-DMBI interaction ($\chi_{N2200/N\text{-}DMBI} > \chi_{PCE10/N\text{-}DMBI} > \chi_{PBDB\text{-}T/N\text{-}DMBI}$). The overall film formation time is determined by in-situ monitoring the film thickness (**Figure S8**). The overall time is similar for PCE10 at 8.5 s and PBDB-T at 8.9 s, comparing with the slow time of 12.7 s for N2200. Rationally, we order the phase separation time between polymer and N-DMBI as $T_{N2200/N\text{-}DMBI} > T_{PCE10/N\text{-}DMBI} > T_{PBDB\text{-}T/N\text{-}DMBI}$. The polymer mobility is related with the viscosity, and it can be assumed according to the solvent/polymer interaction. Since the left side of the tie lines is higher than the right side in CB/PCE10/N-DMBI and CB/PBDB-T/N-DMBI ternary phase diagrams (**Figure 3a** and **b**), CB resides more in polymer donors. The smaller CB/polymer interaction than CB/N-DMBI interaction ($\chi_{CB/polymer} < \chi_{CB/N\text{-}DMBI}$) induces higher polymer mobility with larger droplet collision frequency. In the case of CB/N2200/N-DMBI (**Figure 3c**), the left side of the tie lines is lower than the right side, hence CB resides less in N2200. The swelling effect reduces the mobility of N2200. Since the phase separation time and polymer mobility play opposite roles on polymer/N-DMBI phase separation, we further examined the real morphology

of doped polymer films by contact-mode atomic force microscope (CM-AFM). In the ternary phase diagrams, the solvent quenching lines of 1 wt% N-DMBI doped polymer solutions (the blue arrows) are near the polymer axis, thus we predict that the doped polymer films appear similar morphologies with the pure ones. When we enlarge the doping concentration to 10 wt%, the solvent quenching lines (the orange arrows) enter the meta-stable region, which will lead to pure N-DMBI precipitating from the polymer/N-DMBI mixed phase. The predictions are well confirmed by AFM images in (**Figure 3d-i** and **Figure S9**). Comparing with the neat polymers, we observe the largest phase separation in N2200/N-DMBI film and the smallest one in PBDB-T/N-DMBI film with 10 wt% N-DMBI addition. The observed size of phase separation is well related with the miscibility sequence, demonstrating that the kinetic morphology evolution doesn't change the concise analysis from $\Delta\delta_{i\text{-Hansen}}$ under our experimental conditions. Altogether, the application of miscibility criteria well extends to the solution processed blend films. The ideal n-dopant requires both good miscibility with the acceptor and poor miscibility with the donor in PSCs.

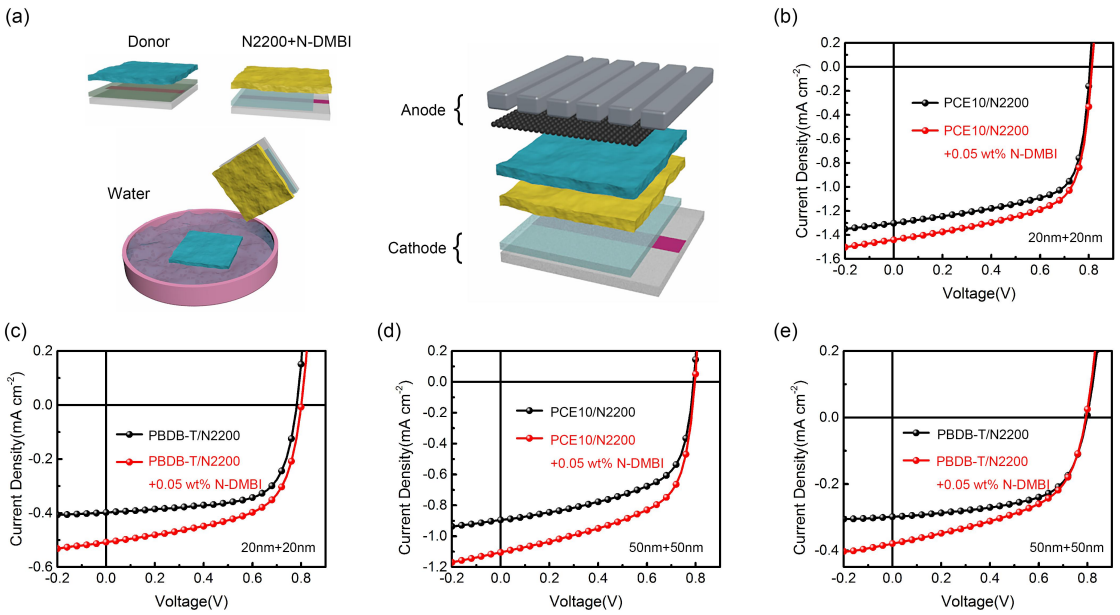

Figure 4. (a) Scheme of the floating-film-transfer method. (b-e) Photovoltaic performances of PHJ devices: (b) *J-V* curves of PCE10/N2200 PHJ devices with 20 nm for each layer; (c) *J-V* curves of PBDB-T/N2200 PHJ devices with 20 nm for each layer; (d) *J-V* curves of PCE10/N2200 PHJ devices with 50 nm for each layer; (e) *J-V* curves of PBDB-T/N2200 PHJ devices with 50 nm for each layer.

PSCs are finally fabricated in the PHJ device structure to locate the N-DMBI in the single component film. The standard PHJ model excludes the morphological variation in the BHJ films of the two polymer blends, which provides the solid evidence for the importance of dopant/component miscibility in efficient n-doped PSCs. PHJ devices were fabricated by the floating-film-transfer method, where the polymer donor layer was stacked onto the N2200 layer. The free-standing polymer donor films were floated on water, and then stacked on the N2200 coated substrates to fabricate the bi-layer blend films (**Figure 4a**). The film thicknesses were selected as 20 nm for each film at first. The *J-V* curves of the 20 nm+20 nm PHJ devices are listed in **Figure 4b** and **c**, as detailed in **Table S3** and **S4**. Interestingly, we observe J_{sc} enhancement in both PCE10/N2200 and PBDB-T/N2200 PHJ devices when adding certain amount of N-DMBI in N2200. At the optimal doping content of 0.05 wt%, the J_{sc} increases from 1.30 mA/cm^2 to 1.44 mA/cm^2 in PCE10/N2200, and similar extent of improvement from 0.40 mA/cm^2 to 0.51 mA/cm^2 is observed in PBDB-T/N2200. We observe no J_{sc} enhancement when N-DMBI is added in PCE10 layer (**Table S5**). The comparison unambiguously reveals that the performance variations in BHJ devices are due to the N-DMBI distribution in different components. We further enlarge the film thickness of single layer to 50 nm. The N-DMBI led J_{sc} enhancement retains in both cases of PHJ devices (**Figure 4d** and **e**, **Table S6** and **S7**). Hence we propose that the performance improvement for n-doped PSCs is independent on the specific morphology in BHJ films, the only requirement is the proper dopant/component miscibility to guarantee the corrected dopant distribution.

CONCLUSION

In summary, we estimate the n-dopant miscibility with both of polymer donor and acceptor according to the Hansen's total solubility parameter. The photovoltaic measurements point out that the efficient n-doping requires selective miscibility to avoid the incorrect dopant distribution in the BHJ film. After excluding the possibility of morphology optimization, we further evaluate the effect of kinetic morphology evolution on dopant distribution by analyzing the ternary phase diagram. Although the film formation time and polymer mobility play opposite roles on dopant/polymer phase separation, the overall result is still consistent with the simple miscibility analysis based on the difference of Hansen's total solubility parameter ($\triangle\delta_{i\text{-}Hansen}$). By confining the n-dopant in the acceptor layer of PHJ devices, J_{sc} enhancement is observed in both of material systems. It unambiguously relates the photovoltaic performance with dopant location, and well supports the assumption in this work. Unlike the single component devices, such as organic field-effect transistor,[17, 46] the PSCs require the selectivity of dopant miscibility in binary BHJ films. Our findings emphasize this long-term neglecting issue, and propose it as an important design rule for effective BHJ doped PSCs. We are optimistic on its general application in high-efficiency material systems and p-doped PSCs.

EXPERIMENTAL SECTION

Materials: PCE10, PBDB-T and N-DMBI were ordered from Solarmer Materials Inc. N2200 was ordered from 1-Materials. Chlorobenzene was purchased from Sigma-Aldrich.

Instrumentation: The apparatus for morphology characterization (AFM and GIWAXS), photovoltaic performance measurements (*J–V* curves, EQE curves and UV–vis absorption spectra), and the film thickness testing are accessible in reference 24 and 28. KPFM images were

obtained from MFP3D (Oxford Instruments, USA). The film formation time was measured by Filmetrics F20-EXR. The contact angle was obtained by KRUSS DSA 100 with water and diiodomethane.

Device fabrication: The PSCs were fabricated in ITO/ZnO/active layer/MoO_x/Ag device structure. The ITO substrates and ZnO layer were cleaned and coated following the steps in reference 47. The blend solutions of PCE10/N2200 and PBDB-T/N2200 were respectively made at a total concentration of 10 mg/mL and 8 mg/mL in CB. Both were made with D/A weight ratio of 1:1. After stirring overnight on a hot plate at 50 °C, a series of doping concentrations relative to N2200 were added to the solutions in four hours before spin-coating the blend films. The PHJ devices were fabricated in a device structure of ITO/ZnO/N2200/Donor/MoO_x/Ag. All of the solutions used possess the same concentration of 6 mg/ml. The floating-film-transfer method were described in reference 24. The anodes of MoO_x and Ag were evaporated as common methods in reference 47. For AFM measurement, the neat and 1 wt% N-DMBI doped polymer films were prepared by adding 1 mg/ml N-DMBI solution in CB to 10 mg/ml polymer solutions in CB. After vigorous stirring at 50 °C for more than 24h, the polymer films were spin-coated on the quartz substrates at 1500 rpm for 40s. The in-situ measurement of film thickness was carried on under the same experimental conditions.

Supporting Information.

The Supporting information is available free of charge on ACS Publication website at DOI:

Computational details about the ternary phase diagrams; Photovoltaic performances of PHJ devices; KPFM images; Contact angle images; EQE dates; GIWAXS patterns; Film formation

time; CM-AFM Graphics; Molecular weight dates; and Ternary phase diagrams calculated by separated Hansen solubility parameters. (PDF)

AUTHOR INFORMATION

Corresponding Author

* E-mail: mseyanhan@xjtu.edu.cn (H.Y.).

* E-mail: msewma@xjtu.edu.cn (W.M.).

Author Contributions

The manuscript was written through contributions of all authors. All authors have given approval to the final version of the manuscript.

Funding Sources

This work was supported by the Ministry of Science and Technology of China, National Natural Science Foundation of China, and the National Science Foundation of Shanxi Province.

Notes

The authors declare no competing financial interest.

ACKNOWLEDGMENT

Thanks for the support from Ministry of science and technology (2016YFA0200700), National Natural Science Foundation of China (21975198, 51803162, 21875182), the Natural Science Foundation of Shanxi Province (2018 JM5007), the Fundamental Research Funds for the Central Universities (Z201805178), and 111 project 2.0 (BP2018008).

ABBREVIATIONS

BHJ, bulk heterojunction

PSCs, polymer solar cells

PBDB-T, poly[(2,6-(4,8-bis(5-(2-ethylhexyl)thiophe-2-yl)-benzo[1,2-b:4,5-b']dithiophene))-alt-(5,5-(1',3'-di-2-thienyl -5',7'-bis(2-ethylhexyl)benzo[1',2'-c:4',5'-c']dithiophene-4,8-dione))]

N2200, poly{[N,N'-bis(2-octyldodecyl)-naphthalene-1,4,5,8-bis(dicarboximide)-2,6-diyl]-alt-5,5'-(2,2'-bithiophene)}

PCE10, poly[4,8-bis(5-(2-ethylhexyl)-thiophene-2-yl)benzo[1,2-b;4,5-b']dithiophene-2,6-diyl-alt-(4-(2-ethylhexyl)-3-fluorothieno[3,4-b]thiophene-)-2-carboxylate-2-6-diyl]]

N-DMBI, (4-(1,3-dimethyl-2,3-dihydro-1H-benzoimidazol-2-yl)phenyl)dimethylamine

PCE, power conversion efficiency

IP, ionization potential

F4TCNQ, 2,3,5,6-tetrafluoro-7,7,8,8-tetracyanoquinodimethane

LUMO, lowest unoccupied molecular orbit

J_{sc}, short-circuit current

PHJ, planar heterojunction

KPFM , Kelvin probe force microscopy

CTC, charge-transfer complex

V_{oc}, open-circuit voltage

FF, fill factor

EQE, external quantum efficiency

TM-AFM, tapping-mode atomic force microscopy

GIWAXS, grazing incident wide-angle X-ray scattering

RMS, root-mean-square

CL, coherence length

CB, chlorobenzene

GPC, gel permeation chromatography

CM-AFM, contact mode atomic force microscope

REFERENCES

(1) Yu, G.; Gao, J.; Hummelen, J. C.; Wudl, F.; Heeger, A. J. Polymer Photovoltaic Cells - Enhanced Efficiencies via a Network of Internal Donor-Acceptor Heterojunctions. *Science* **1995**, *270*, 1789-1791.

(2) Halls, J. J. M.; Walsh, C. A.; Greenham, N. C.; Marseglia, E. A.; Friend, R. H.; Moratti, S. C.; Holmes, A. B. Efficient Photodiodes from Interpeneprating Polymer Networks. *Nature* **1995**, *376*, 498-500.

(3) Yu, R.; Yao, H.; Cui, Y.; Hong, L.; He, C.; Hou, J. Improved Charge Transport and Reduced Nonradiative Energy Loss Enable Over 16% Efficiency in Ternary Polymer Solar Cells. *Adv. Mater.* **2019,** *31*, 1902302.

(4) Hou, J.; Inganas, O.; Friend, R. H.; Gao, F. Organic Solar Cells Based on Non-Fullerene Acceptors. *Nat. Mater.* **2018,** *17*, 119-128.

(5) Yan, C.; Barlow, S.; Wang, Z.; Yan, H.; Jen, A. K. Y.; Marder, S. R.; Zhan, X. Non-Fullerene Acceptors for Organic Solar Cells. *Nat. Rev. Mater.* **2018,** *3*, 18003.

(6) Zhang, J.; Tan, H. S.; Guo, X.; Facchetti, A.; Yan, H. Material Insights and Challenges for Non-Fullerene Organic Solar Cells Based on Small Molecular Acceptors. *Nat. Energy* **2018,** *3*, 720-731.

(7) Zhao, F.; Wang, C.; Zhan, X. Morphology Control in Organic Solar Cells. *Adv. Energy Mater.* **2018,** *8*, 1703147.

(8) Kang, H.; Lee, W.; Oh, J.; Kim, T.; Lee, C.; Kim, B. J. From Fullerene-Polymer to All-Polymer Solar Cells: The Importance of Molecular Packing, Orientation, and Morphology Control. *Acc. Chem. Res.* **2016,** *49*, 2424-2434.

(9) Lee, H.; Park, C.; Sin, D. H.; Park, J. H.; Cho, K. Recent Advances in Morphology Optimization for Organic Photovoltaics. *Adv. Mater.* **2018,** *30*, 1800453.

(10) Sun, C.; Wu, Z.; Hu, Z.; Xiao, J.; Zhao, W.; Li, H.-W.; Li, Q.-Y.; Tsang, S.-W.; Xu, Y.-X.; Zhang, K.; Yip, H.-L.; Hou, J.; Huang, F.; Cao, Y. Interface Design for High-Efficiency Non-Fullerene Polymer Solar Cells. *Energy Environ. Sci.* **2017,** *10*, 1784-1791.

(11) Yin, Z.; Wei, J.; Zheng, Q. Interfacial Materials for Organic Solar Cells: Recent Advances and Perspectives. *Adv. Sci.* **2016,** *3*, 1500362.

(12) Kang, Q.; Ye, L.; Xu, B.; An, C.; Stuard, S. J.; Zhang, S.; Yao, H.; Ade, H.; Hou, J. A Printable Organic Cathode Interlayer Enables over 13% Efficiency for 1-cm^2 Organic Solar Cells. *Joule* **2019,** *3*, 227-239.

(13) Gaul, C.; Hutsch, S.; Schwarze, M.; Schellhammer, K. S.; Bussolotti, F.; Kera, S.; Cuniberti, G.; Leo, K.; Ortmann, F. Insight into Doping Efficiency of Organic Semiconductors from the Analysis of the Density of States in N-Doped C-60 and ZnPc. *Nat. Mater.* **2018,** *17*, 439-444.

(14) Schwarze, M.; Tress, W.; Beyer, B.; Gao, F.; Scholz, R.; Poelking, C.; Ortstein, K.; Guenther, A. A.; Kasemann, D.; Andrienko, D.; Leo, K. Band Structure Engineering in Organic Semiconductors. *Science* **2016,** *352*, 1446-1449.

(15) Schwarze, M.; Gaul, C.; ScholZ, R.; Bussolotti, F.; Hofacker, A.; Schellhammer, K. S.; Nell, B.; Naab, B. D.; Bao, Z.; Spoltore, D.; Vandewal, K.; Widmer, J.; Kera, S.; Ueno, N.; Ortmann, F.; Leo, K. Molecular Parameters Responsible for Thermally Activated Transport in Doped Organic Semiconductors. *Nat. Mater.* **2019,** *18*, 242-248.

(16) Sun, L.; Sun, J.-X.; Xiong, C.-H.; Shi, X.-H. Trap-Assisted Recombination in Disordered Organic Semiconductors Extended by Considering Density Dependent Mobility. *Sol. Energy* **2016,** *135*, 308-316.

(17) Xu, Y.; Sun, H.; Liu, A.; Zhu, H.-H.; Li, W.; Lin, Y.-F.; Noh, Y.-Y. Doping: A Key Enabler for Organic Transistors. *Adv. Mater.* **2018,** *30*, 1801830.

(18) Paterson, A. F.; Tsetseris, L.; Li, R.; Basu, A.; Faber, H.; Emwas, A.-H.; Panidi, J.; Fei, Z.; Niazi, M. R.; Anjum, D. H.; Heeney, M.; Anthopoulos, T. D. Addition of the Lewis Acid Zn(C_6

$F_5)_2$ Enables Organic Transistors with a Maximum Hole Mobility in Excess of 20 cm^2 V^{-1} s^{-1}. *Adv. mater.* **2019**, 1900871.

(19) Higgins, A.; Mohapatra, S. K.; Barlow, S.; Marder, S. R.; Kahn, A. Dopant Controlled Trap-Filling and Conductivity Enhancement in an Electron-Transport Polymer. *Appl. Phys. Lett.* **2015,** *106*, 163301.

(20) Tietze, M. L.; Pahner, P.; Schmidt, K.; Leo, K.; Luessem, B. Doped Organic Semiconductors: Trap-Filling, Impurity Saturation, and Reserve Regimes. *Adv. Funct. Mater.* **2015,** *25*, 2701-2707.

(21) Olthof, S.; Mehraeen, S.; Mohapatra, S. K.; Barlow, S.; Coropceanu, V.; Bredas, J.-L.; Marder, S. R.; Kahn, A. Ultralow Doping in Organic Semiconductors: Evidence of Trap Filling. *Phys. Rev. Lett.* **2012,** *109*, 176601.

(22) Shang, Z.; Heumueller, T.; Prasanna, R.; Burkhard, G. F.; Naab, B. D.; Bao, Z.; McGehee, M. D.; Salleo, A. Trade-Off between Trap Filling, Trap Creation, and Charge Recombination Results in Performance Increase at Ultralow Doping Levels in Bulk Heterojunction Solar Cells. *Adv. Energy Mater.* **2016,** *6*, 1601149.

(23) Deschler, F.; Da Como, E.; Limmer, T.; Tautz, R.; Godde, T.; Bayer, M.; von Hauff, E.; Yilmaz, S.; Allard, S.; Scherf, U.; Feldmann, J. Reduced Charge Transfer Exciton Recombination in Organic Semiconductor Heterojunctions by Molecular Doping. *Phys. Rev. Lett.* **2011,** *107*, 127402.

(24) Yan, H.; Tang, Y.; Sui, X.; Liu, Y.; Gao, B.; Liu, X.; Liu, S. F.; Hou, J.; Ma, W. Increasing Quantum Efficiency of Polymer Solar Cells with Efficient Exciton Splitting and Long Carrier Lifetime by Molecular Doping at Heterojunctions. *ACS Energy Lett.* **2019,** *4*, 1356-1363.

(25) Yan, H.; Manion, J. G.; Yuan, M.; de Arquer, F. P. G.; McKeown, G. R.; Beaupre, S.; Leclerc, M.; Sargent, E. H.; Seferos, D. S. Increasing Polymer Solar Cell Fill Factor by Trap-Filling with F4-TCNQ at Parts Per Thousand Concentration. *Adv. Mater.* **2016,** *28*, 6491-6496.

(26) Yu, S.; Frisch, J.; Opitz, A.; Cohen, E.; Bendikov, M.; Koch, N.; Salzmann, I. Effect of Molecular Electrical Doping on Polyfuran Based Photovoltaic Cells. *Appl. Phys. Lett.* **2015,** *106*, 203301.

(27) Han, X.; Wu, Z.; Sun, B. Enhanced Performance of Inverted Organic Solar Cell by a Solution-Based Fluorinated Acceptor Doped P3HT:PCBM Layer. *Org. Electron.* **2013,** *14*, 1116-1121.

(28) Yan, H.; Chen, J.; Zhou, K.; Tang, Y.; Meng, X.; Xu, X.; Ma, W. Lewis Acid Doping Induced Synergistic Effects on Electronic and Morphological Structure for Donor and Acceptor in Polymer Solar Cells. *Adv. Energy Mater.* **2018,** *8*, 1703672.

(29) Xiong, Y.; Ye, L.; Gadisa, A.; Zhang, Q.; Rech, J. J.; You, W.; Ade, H. Revealing the Impact of F4-TCNQ as Additive on Morphology and Performance of High-Efficiency Nonfullerene Organic Solar Cells. *Adv. Funct. Mater.* **2019,** *29*, 1806262.

(30) Xu, Y.; Yuan, J.; Sun, J.; Zhang, Y.; Ling, X.; Wu, H.; Zhang, G.; Chen, J.; Wang, Y.; Ma, W. Widely Applicable N-Type Molecular Doping for Enhanced Photovoltaic Performance of All-Polymer Solar Cells. *ACS Appl. Mater. Interfaces* **2018,** *10*, 2776-2784.

(31) Lin, X.; Wegner, B.; Lee, K. M.; Fusella, M. A.; Zhang, F.; Moudgil, K.; Rand, B. P.; Barlow, S.; Marder, S. R.; Koch, N.; Kahn, A. Beating the Thermodynamic Limit with Photo-Activation of N-Doping in Organic Semiconductors. *Nat. Mater.* **2017,** *16*, 1209-1215.

(32) Gao, W. Y.; Kahn, A. Controlled P-Doping of Zinc Phthalocyanine by Coevaporation with Tetrafluorotetracyanoquinodimethane: A Direct and Inverse Photoemission Study. *Appl. Phys. Lett.* **2001,** *79*, 4040-4042.

(33) Yan, H.; Tang, Y.; Meng, X.; Xiao, T.; Lu, G.; Ma, W. Achieving High Doping Concentration by Dopant Vapor Deposition in Organic Solar Cells. *ACS Appl. Mater. Interfaces* **2019,** *11*, 4178-4184.

(34) Jacobs, I. E.; Moule, A. J. Controlling Molecular Doping in Organic Semiconductors. *Adv. Mater.* **2017,** *29*,1703063.

(35) Ye, L.; Hu, H.; Ghasemi, M.; Wang, T.; Collins, B. A.; Kim, J.-H.; Jiang, K.; Carpenter, J. H.; Li, H.; Li, Z.; McAfee, T.; Zhao, J.; Chen, X.; Lai, J. L. Y.; Ma, T.; Bredas, J.-L.; Yan, H.; Ade, H. Quantitative Relations between Interaction Parameter, Miscibility and Function in Organic Solar Cells. *Nat. Mater.* **2018,** *17*, 253-260.

(36) Ye, L.; Collins, B. A.; Jiao, X.; Zhao, J.; Yan, H.; Ade, H. Miscibility-Function Relations in Organic Solar Cells: Significance of Optimal Miscibility in Relation to Percolation. *Adv. Energy Mater.* **2018,** *8*, 1703058.

(37) Ye, L.; Li, S.; Liu, X.; Zhang, S.; Ghasemi, M.; Xiong, Y.; Hou, J.; Ade, H. Quenching to the Percolation Threshold in Organic Solar Cells. *Joule* **2019,** *3*, 443-458.

(38) Jacobs, I. E.; Aasen, E. W.; Oliveira, J. L.; Fonseca, T. N.; Roehling, J. D.; Li, J.; Zhang, G.; Augustine, M. P.; Mascal, M.; Moulé, A. J. Comparison of Solution-Mixed and Sequentially Processed P3HT:F4TCNQ Films: Effect of Doping-Induced Aggregation on Film Morphology. *J.Mater. Chem. C*, **2016**, *4*, 3454-3466.

(39) Duong, D. T.; Wang, C.; Antono, E.; Toney, M. F.; Salleo, A. The Chemical and Structural Origin of Efficient p-Type Doping in P3HT. *Organic Electronics* **2013**, *14*, 1330–1336.

(40) Hexemer, A.; Bras, W.; Glossinger, J.; Schaible, E.; Gann, E.; Kirian, R.; MacDowell, A.; Church, M.; Rude, B.; Padmore, H. A SAXS/WAXS/GISAXS Beamline with Multilayer Monochromator. *J.Phys. Conf. Ser.* **2010**, *247*, 012007.

(41) Duong, D. T.; Phan, H.; Hanifi, D.; Jo, P. S.; Nguyen, T. Q.; Salleo, A. Direct Observation of Doping Sites in Temperature-Controlled, P-Doped P3HT Thin Films by Conducting Atomic Force Microscopy. *Adv. Mater.* **2014**, *26*, 6069–6073.

(42) Yilmaz, L.; McHugh, A. J. Analysis of Nonsolvent-Solvent-Polymer Phase-Diagrams and Their Relevance to Membrane Formation Modeling. *J. Appl. Polym. Sci.* **1986,** *31*, 997-1018.

(43) Kouijzer, S.; Michels, J. J.; van den Berg, M.; Gevaerts, V. S.; Turbiez, M.; Wienk, M. M.; Janssen, R. A. J. Predicting Morphologies of Solution Processed Polymer:Fullerene Blends. *J. Am. Chem. Soc.* **2013,** *135*, 12057-12067.

(44) Kim, J.-H.; Gadisa, A.; Schaefer, C.; Yao, H.; Gautam, B. R.; Balar, N.; Ghasemi, M.; Constantinou, I.; So, F.; O'Connor, B. T.; Gundogdu, K.; Hou, J.; Ade, H. Strong Polymer

Molecular Weight-Dependent Material Interactions: Impact on the Formation of the Polymer/Fullerene Bulk Heterojunction Morphology. *J. Mater. Chem. A* **2017,** *5*, 13176-13188.

(45) Bokel, F. A.; Engmann, S.; Herzing, A. A.; Collins, B. A.; Ro, H. W.; DeLongchamp, D. M.; Richter, L. J.; Schaible, E.; Hexemer, A. In Situ X-ray Scattering Studies of the Influence of an Additive on the Formation of a Low-Bandgap Bulk Heterojunction. *Chem. Mater.* **2017,** *29*, 2283-2293.

(46) Lussem, B.; Keum, C.-M.; Kasemann, D.; Naab, B.; Bao, Z.; Leo, K. Doped Organic Transistors. *Chem. Rev.* **2016,** *116*, 13714-13751.

(47) Zhang, L.; Lin, B.; Ke, Z.; Chen, J.; Li, W.; Zhang, M.; Ma, W. A Universal Approach to Improve Electron Mobility without Significant Enlarging Phase Separation in IDT-Based Non-Fullerene Acceptor Organic Solar Cells. *Nano Energy* **2017,** *41*, 609-617.